Cell, Vol. 116, 577–589, February 20, 2004, Copyright ©2004 by Cell Press

Nanoscale Organization of Multiple GPI-Anchored Proteins in Living Cell Membranes

Pranav Sharma,[1,4] Rajat Varma,[1,4,5] R.C. Sarasij,[2,4] Ira,[3,6] Karine Gousset,[6] G. Krishnamoorthy,[3] Madan Rao,[1,2,*] and Satyajit Mayor[1,*]

[1]National Centre for Biological Science (TIFR)
UAS-GKVK Campus
GKVK PO
Bangalore 560 065
India

[2]Raman Research Institute
CV Raman Avenue
Bangalore 560 080
India

[3]Department of Chemical Sciences
Tata Institute of Fundamental Research (TIFR)
Homi Bhabha Road
Mumbai 400005
India

Summary

Cholesterol and sphingolipid-enriched "rafts" have long been proposed as platforms for the sorting of specific membrane components including glycosylphosphatidylinositol-anchored proteins (GPI-APs), however, their existence and physical properties have been controversial. Here, we investigate the size of lipid-dependent organization of GPI-APs in live cells, using homo and hetero-FRET-based experiments, combined with theoretical modeling. These studies reveal an unexpected organization wherein cell surface GPI-APs are present as monomers and a smaller fraction (20%–40%) as nanoscale (<5 nm) cholesterol-sensitive clusters. These clusters are composed of at most four molecules and accommodate diverse GPI-AP species; crosslinking GPI-APs segregates them from preexisting GPI-AP clusters and prevents endocytosis of the crosslinked species via a GPI-AP-selective pinocytic pathway. In conjunction with an analysis of the statistical distribution of the clusters, these observations suggest a mechanism for functional lipid-dependent clustering of GPI-APs.

Introduction

Rafts have been hypothesized as lateral heterogeneities in membranes of living cells that are enriched in (glyco) sphingolipids, cholesterol, and specific membrane proteins. They have been proposed to be responsible for the sorting of associated proteins and for providing sites for the assembly of cytoplasmic signaling complexes in a variety of biological contexts (Anderson and Jacobson, 2002; Jacobson and Dietrich, 1999; Simons and Ikonen, 1997; Simons and Toomre, 2000). Two major hypotheses regarding the nature of cell membrane rafts are: (1) rafts are relatively large (>50 nm) cholesterol and sphingolipid-rich structures wherein associated proteins are likely to be concentrated (Simons and Ikonen, 1997; Simons and Toomre, 2000), (2) rafts are dynamic assemblies of small size, constituted by components that are preferentially associated with lipids; functional organization is dictated by the induction of stable large-scale structures (Anderson and Jacobson, 2002).

The prevailing operational description of rafts is based on the observation that detergent-resistant membranes (DRMs) obtained by the extraction of living cells with cold nonionic detergents (e.g. Triton X-100), retain a specific set of proteins and lipids, including GPI-anchored proteins (GPI-APs), signaling proteins such as lipid-linked nonreceptor tyrosine kinases, (glyco)sphingolipids, and cholesterol (Brown and London, 2000). DRM-association has also been shown to correlate with the sorting and signaling properties of some proteins (Brown and London, 2000; Simons and Ikonen, 1997; Simons and Toomre, 2000). More recently however, the correlation of DRMs with preexisting lipid domains in membranes is being seriously contested. For instance, in homogeneous fluid membrane systems, Triton X-100 treatment was found to induce large-scale ordered domains (Heerklotz, 2002) and in some cases the addition of the detergent severely perturbs preexisting l_o domains (Heerklotz et al., 2003). Consequently, in the more complex environment of the cell membrane, DRM-association should not be relied upon to provide information regarding any kind of preexisting organization of components (Zurzolo et al., 2003). Thus, new methodologies are necessary for establishing the existence and properties of in vivo rafts involved in cellular function.

Here, we focus on the cell surface organization of a common raft-marker, GPI-APs, which are a diverse set of exoplasmic, eukaryotic proteins exhibiting specific intracellular sorting and signaling properties regulated by alterations in cholesterol and sphingolipid levels in cell membranes (Chatterjee and Mayor, 2001; Mayor and Riezman, 2004). The lipid-dependent organization of GPI-APs at the cell surface will directly reveal the structure of rafts and establish a direct functional significance for this concept.

While experiments on artificial membrane containing a lipid composition resembling that of DRMs exhibit ordered domains with sizes ranging from the nanometer to the micron scale (Silvius, 2003), both fluorescence microscopy and conventional electron microscopy have consistently failed to reveal large-scale laterally segregated structures enriched in GPI-APs in living cells (Hao et al., 2001; Mayor and Maxfield, 1995; Mayor et al., 1994; Parton et al., 1994); viewed at optical resolution (~400 nm), GPI-APs appear uniformly distributed in cell membranes. Thus, if cellular rafts exist they are likely to be small and/or extremely dynamic.

In native cell membranes, methods designed to detect

*Correspondence: madan@rri.res.in (M.R.), mayor@ncbs.res.in (S.M)
[4]These authors contributed equally to this work.
[5]Present address: Program in Molecular Pathogenesis, Skirball Institute for Biomolecular Medicine, New York University School of Medicine, 540 First Avenue, New York, New York 10016.
[6]Present address: Department of Biology, Johns Hopkins University, 3400 North Charles Street, Baltimore, Maryland 21218.

proximity between molecules have observed inhomogeneous distributions of GPI-APs. Chemical crosslinking with short (1.1 nm) crosslinkers indicate that cholesterol-sensitive complexes of GPI-APs exist at the cell surface (Friedrichson and Kurzchalia, 1998). Using a fluorescence resonance energy transfer (FRET) method called homo-FRET which detects proximity between like fluorophores at 1–10 nm scale we had suggested that GPI-APs occur in cholesterol-sensitive, submicron-sized "domains" at the surface of living cells (Varma and Mayor, 1998). In contrast, studies based on detecting FRET between different fluorophores (hetero-FRET) reported the absence of detectable clustering of GPI-APs, putting an upper bound on the fraction (if any) of clustered GPI-APs (Kenworthy and Edidin, 1998; Kenworthy et al., 2000). Alternative approaches to look for rafts in cell membranes have relied on single particle tracking measurements. Even here there appears to be a remarkable lack of consensus on the existence, size, lifetime, and structure of lipid-dependent assemblies (reviewed in Subczynski and Kusumi, 2003).

To investigate the structure of lipid-dependent assemblies of GPI-APs in live cells at a spatial scale below optical resolution we have once again used homo-FRET microscopy to study the organization of different GPI-APs expressed in multiple cell lines (see Figure 1A). We have extended our earlier steady-state methods by theoretically modeling the changes observed in homo-FRET efficiencies upon photobleaching the fluorophores to provide information about the size of the GPI-AP containing structures, in conjunction with direct measurements of anisotropy decay rates to determine intermolecular distances in the cluster. In addition, we have revisited the hetero-FRET experiments with additional theoretical analyses. Together, the experiments and theoretical analyses reveal an unexpected nanometer scale organization of GPI-APs, wherein 20%–40% of GPI-APs are organized as clusters consisting of at most four molecules and the remaining are present as monomers. We provide evidence that these clusters are sensitive to cholesterol depletion, that multiple GPI-APs cohabit the same cluster and that crosslinking perturbs the preexisting organization. Our data also indicate that organization at this scale is necessary for the specific endocytic sorting displayed by GPI-APs.

Results

Experimental Strategy to Study the Nature of Organization of Cell Surface GPI-APs

We have principally used homo-FRET microscopy to determine the size and structure of GPI-AP organization. Homo-FRET is measured by monitoring the extent of depolarization of fluorescence emission over and above that produced by rotational diffusion of the fluorophores (Figure 1B; see also explanation in Supplemental Data, Supplemental Figure S1 available at http://www.cell.com/cgi/content/full/116/4/577/DC1). As earlier, we estimated homo-FRET between GPI-APs by measuring the fluorescence emission anisotropy of these proteins at the surface of living cells. First, we extend the steady-state homo-FRET measurements to different GPI-APs (principally GFP-GPI and variants of the GFP fluorophore; Figure 1A) to show clustered distribution of diverse GPI-APs in multiple cell lines. Second, time resolved anisotropy decay experiments provide evidence of high density in clusters. Third, steady-state anisotropy as a function of photobleaching, in conjunction with a detailed theoretical analysis suggests that these dense clusters are small and only a fraction of GPI-APs are clustered. Finally, theoretical modeling of hetero-FRET measurements confirm the presence of a fraction of small, dense clusters. We have kept the analytical methods used for these experiments in a single location (Supplemental Data available on *Cell* website), thus, if the reader wishes to obtain the details of these calculations they are urged to refer to this section.

Diverse GPI-APs Are Present as Clusters at the Cell Surface

At optical microscopy resolution, GFP-GPI (Figure 1C), mYFP-GPI, and mCFP-GPI (data not shown) exhibited a diffuse distribution at the surface of live cells; based on the maximum intensity of GFP-GPI, this corresponds to a maximum of $\sim$400 GFP-fluorophores/μm^2 on the cell surface (Supplemental Data available on *Cell* website). If these molecules are distributed uniformly, the typical interprotein distance would be at least $\sim$50 nm, much too large for any energy transfer (Forster radius of GFP $R_0 = 4.65$ nm, Patterson et al., 2000). At these separations, we expect an anisotropy close to its value at infinite dilution in the membrane ($A_\infty = 0.315$ for GFP-GPI in CHO cells; see Supplemental Data available on *Cell* website). However, upon excitation by polarized light, GFP-GPI exhibited fluorescence anisotropy values (0.295 ± 0.005), which were significantly lower, indicating significant fluorescence depolarization. Even so, the fluorescence anisotropy has a constant value over the entire fluorescence intensity range (Figures 1C–1E). Similar observations have been made with GFP-GPI in MDCK cells, mCFP-GPI (data not shown), and mYFP-GPI (Figure 1F) in CHO cells.

The reduced anisotropy observed for GFP-GPI and mYFP-GPI may be either due to homo-FRET and/or due to increased rotational mobility. By directly measuring the rates of anisotropy decay at picosecond time scales, we can resolve the respective contributions of homo-FRET and of rotational mobility (see Figure 1B). Time-resolved anisotropy decays of GFP-GPI (Figure 1H: green line) and mYFP-GPI (Figure 1I: green line) in living cells at the picosecond scale exhibited both a fast (Table 1; τ_{r1}) and a slow decay (Table 1; τ_{r2}) component for the two proteins. The slow decay component is due to rotational diffusion of the membrane-tethered protein since it was eliminated by placing the cells in a highly viscous medium (50% glycerol: Figure 1G, green line); we also note that the slow decay component of GFP-GPI is much longer than the measured rotational correlation time of a freely diffusible molecule of similar size (29 kDa; Table 1). The fast decay component then is due to FRET since: (1) it was absent in GFP molecules in free solution (Figure 1G; black line) and in PI-PLC released GFP or mYFP molecules from GFP- or mYFP-GPI expressing cells, respectively, where they are beyond FRET range (Table 1); (2) it is present upon crosslinking of GFP monomers with glutaraldehyde (Figure 1G; red

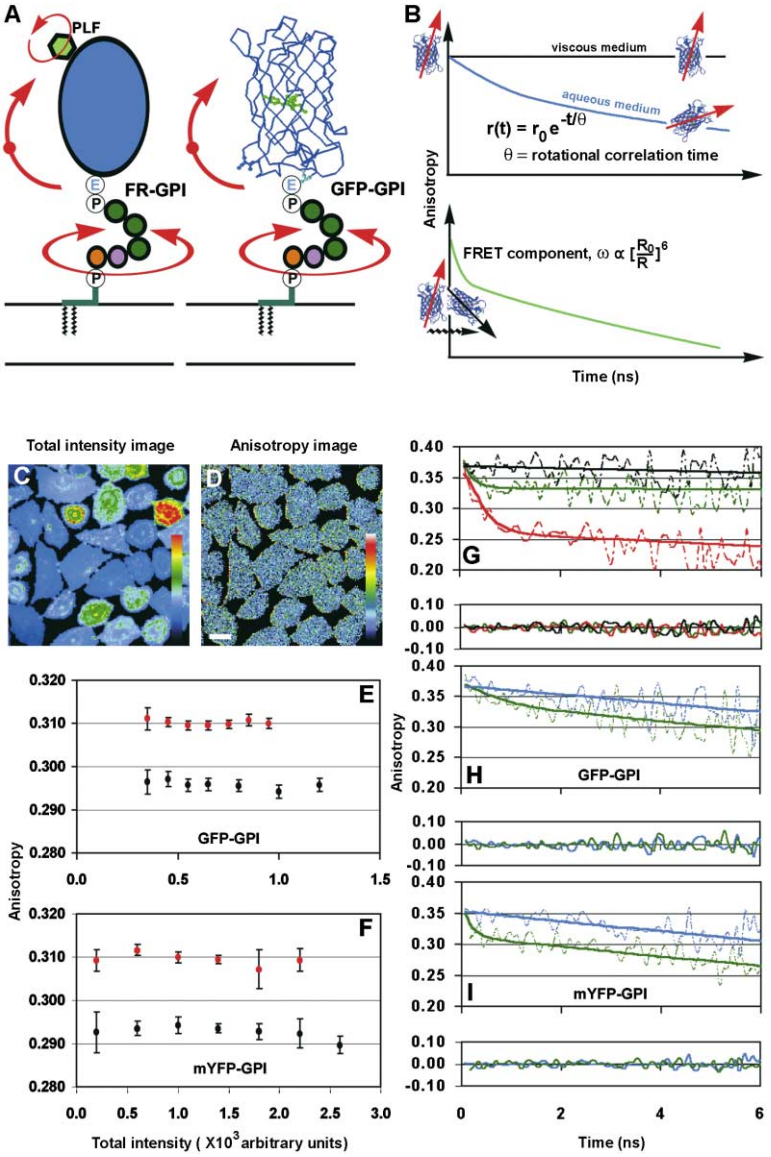

Figure 1. GFP-GPI Exhibits Concentration-Independent FRET at the Surface of Living Cells

(A) shows cartoons depicting the possibilities of rotational motion (red arrows) for the fluorophores, PLF-FR-GPI {human folate receptor (FR-GPI) labeled via a monovalent fluorescent folic acid analog, N-α-pteroyl-N-ε-(4′-fluorescein-thiocarbamoyl)-L-lysine (PLF)}, GPI-anchored enhanced green fluorescent protein (GFP-GPI) and variants of GFP, mCFP- and mYFP-GPI.

(B) shows the expected time-resolved anisotropy decay profiles for dilute GFP-fluorophores (top) immobilized in glycerol solution (viscous medium, black line) or freely rotating in an aqueous solution (blue line). Fluorophores undergoing FRET (green line, bottom) have an additional fast anisotropy decay rate, ω. Total intensity (C) and anisotropy (D) images of a single field of GG8Tb-1 cells expressing GFP-GPI are shown as pseudocolored 8-bit images. Mean fluorescence emission anisotropy of GFP-GPI (E) or mYFP-GPI (F) expressing cells under normal (black circles) and cholesterol depleted (red circles) conditions were obtained for cells with different intensity ranges (±150 units) and plotted against the midpoint of the interval. Each data point in (E) and (F) is the weighted means from two independent determinations, each consisting of 4–40 cells per interval; vertical bars represent errors in the estimation of the mean. Note that both GFP-GPI and mYFP-GPI exhibit concentration independent anisotropy that is altered by cholesterol depletion using saponin treatment. The LUT bar in (C) represents a linear scale of fluorescence intensity of arbitrary units from 450 (blue) to 2000 (red) intensity corresponding to those shown in (E). The LUT bar in (D) represents a linear scale of anisotropy ranging from 0.3 (blue) to 0.45 (white).

Time resolved anisotropy decay profiles (G) for GFP in 60% glycerol (dashed black line), glutaraldehyde crosslinked GFP in 60% glycerol (dashed red line) and GFP-GPI on surface of cells placed in 50% glycerol (dashed green line) are shown along with their corresponding best-fits (thick lines; see Table 1 for fit parameters) and residuals in the same color code.

(H) and (I) show time resolved anisotropy decays of GFP-GPI (H) and mYFP-GPI (I) expressed on surface of CHO cells, with (dashed blue line) or without (dashed green line) saponin treatment to deplete cholesterol. Corresponding best fits (represented with thick lines; see Table 1 for fit parameters) and residuals are provided in same color code. Note that GFP-GPI and mYFP undergo efficient homo-FRET resulting in a rapid component in the decay of anisotropy that is absent after saponin-treatment. Scale bar is equal to 30 μm.

line); (3) it is insensitive to increase in viscosity of the medium surrounding the cell (Figure 1G; green line); and (4) it occurs at rates that are much faster than the lifetime of fluorophores, consistent with FRET processes (Clayton et al., 2002; Gautier et al., 2001; Tanaka and Mataga, 1979). Consistent with FRET, reducing the density of fluorophores by chemical quenching results in an increase in the steady-state anisotropy of GFP-GPI (Supplemental Figure S1C available on *Cell* website). To conclude, the various GPI-AP species are clustered on the cell surface and undergo significant homo-FRET: this comes from the presence of a fast decay component in the time-resolved anisotropy and significant reduction in steady-state anisotropy.

We rule out that FRET between GPI-AP species is a result of protein-protein interactions; of particular concern is the intrinsic oligomerization potential of GFP as suggested by Zacharias et al. (2002). For this purpose, we compared GFP-GPI and mYFP-GPI where specific residues have been mutated to abolish oligomerization of the YFP fluorophore (Zacharias et al., 2002). We find that FRET between the GPI-AP species requires the GPI-anchor and cholesterol, requirements that are inconsistent with self-oligomerization in membranes. This follows from (1) cholesterol-depletion of GFP-GPI and mYFP-GPI expressing cells by extraction with saponin (Figures 1E and 1F) resulted in a complete loss of the homo-FRET (fast) component (Table 1; Figures 1H, and 1I, blue traces) and a concomitant increase of steady-state anisotropy (Figures 1E and 1F; red circles), and

Table 1. Anisotropy Decay Parameters of GFP, GFP-GPI, mYFP-GPI, and GFP-PIT Expressed on CHO cells[d]

		Anisotropy Decay Times[c] (τ_r in nsec)		Interprotein Distances (in nm)	
	Protein	τ_{r1}	τ_{r2}	Forster's radius (R_0)[f]	Interfluorophore distance (R)[g]
1	GFP in PBS	14.7 ± 0.7			
2	Crosslinked GFP[a]	0.3 ± 0.06 (0.3 ± 0.04)	>40 (0.7 ± 0.04)	4.65 ± 0.09	3.85 ± 0.2
3	GFP-GPI	0.23 ± 0.11 (0.09 ± 0.01)	>25 (0.91 ± 0.04)	4.65 ± 0.09	**3.53 ± 0.46**
4	GFP-GPI (saponin[b])	40 ± 5.0			
5	GFP-PIT	50 ± 4.0			
6	mYFP (PIPLC[e])	17.2 ± 0.9			
7	mYFP-GPI	0.132 ± 0.05 (0.1 ± 0.004)	>35 (0.9 ± 0.004)	4.96 ± 0.1	**3.34 ± 0.33**
8	mYFP-GPI (saponin[b])	42 ± 4.0			

[a] GFP was quantitatively crosslinked with 0.25% glutaraldehyde in phosphate buffered saline, pH 7.4. Time-resolved experiments were conducted in 60% glycerol (Supplemental Figure S1 available on *Cell* website). Fluorescence life times of crosslinked GFP in 60% glycerol are similar to monomeric GFP in 60% glycerol.

[b] Cells were treated with 0.2% saponin for 30 min on ice.

[c] τ_r values represent average from 6–9 fields consisting of 2–3 cells each; amplitudes of the individual components are normalized to one and shown in parenthesis. (Fluorescence lifetimes for each condition have been independently determined from 2–6 fields in each case and shown in Supplemental Data available on *Cell* website).

[d] In all cases, cells were treated with cycloheximide for 3 hr prior to imaging to remove Golgi-associated fluorescence. (Sabharanjak et al., 2002)

[e] CHO cells expressing mYFP-GPI were treated with PIPLC (on ice) to obtain mYFP in phosphate-buffered saline, pH 7.4.

[f] Forster's radii were directly taken from (Patterson et al., 2000); R_0 for YFP was corrected for the experimentally determined extinction coefficient (ϵ) at pH 7.4, which was 0.85 that obtained at pH 8.0.

[g] Interfluorophore distances R, were calculated according to (Gautier et al., 2001) as described in Experimental Procedures.

(2) both steady-state and time-resolved anisotropy measurements showed that the reduced anisotropy due to FRET was abolished by replacement of the GPI-anchor on GFP-GPI with a transmembrane anchor (GFP-PIT; Table 1). Furthermore, unlike the wild-type YFP protein (Zacharias et al., 2002), GFP molecules in solution do not show any evidence of oligomerization (see Supplemental Data available on *Cell* website).

Thus, we detect robust homo-FRET between molecules of diverse GPI-APs in living cell membranes. Given the average concentration of GPI-AP species in membranes, this is indicative of a clustered distribution below optical resolution. The clustering of GPI-APs seems to be promoted by the GPI-anchor.

GPI-APs Are Present in Extremely High-Density Structures

FRET efficiencies between different fluorophores (hetero-FRET) have been used to obtain information regarding intermolecular distances at the nanometer scale (Stryer and Haugland, 1978). Likewise, homo-FRET efficiencies can be used to obtain similar information by the measurement of the rate of loss of fluorescence anisotropy (ω; see Figure 1B) at subnanosecond time domains (Figure 1B). The decay rate is a sensitive measure of the distance between fluorophores undergoing FRET; faster rates are indicative of shorter intermolecular distances (Gautier et al., 2001). Rapid loss of GFP-anisotropy (0.23 ± 0.11 nsec; Table 1; Figure 1H) shows that at least a fraction (>10%) of GFP-GPI species are organized in extremely high-density structures with intermolecular separation of 3.53 ± 0.455 nm (Table 1). For comparison, we produced an artificially clustered GFP organization by crosslinking GFP monomers with glutaraldehyde (a 0.3 nm crosslinker); this also exhibited a fast anisotropy decay component (0.3 ± 0.06; Figure 1G, Table 1) corresponding to an interfluorophore distance of 3.85 ± 0.2 nm (Table 1). Experiments conducted on mYFP-GPI (Figure 1I; green trace) show that the decay rate is even shorter (τ_{r1} = 0.132 ± 0.05) than that observed for GFP-GPI (Table 1). This is entirely consistent with the larger value of R_0 for homo-FRET between two YFP molecules (Patterson et al., 2000), and corresponds to inter-YFP fluorophore distance indistinguishable from the GFP-GPI counterpart (Table 1). Time-resolved anisotropy measurements on PLF-labeled FR-GPI (PLF-FR-GPI) on the surface of CHO cells also reflect a similar high-density organization of FR-GPIs (see Supplemental Data, Supplemental Figure S2 available on *Cell* website). Thus the attachment of a GPI-anchor is capable of organizing diverse proteins into cholesterol-dependent high-density structures with interfluorophore distances <4 nm.

GPI-APs Form Nanometer-Sized Clusters at the Cell Surface

To determine the size of these high-density structures, we devised a methodology based on the observation that the extent of homo-FRET and thus, the steady state anisotropy changes in a theoretically predictable manner (Agranovich and Galanin, 1982; see also Supplemental Data available on *Cell* website) with changes in concentration of fluorophores in a particular structure. We first verified this concept in our experimental setup. Thus increasing concentrations of lissamine rhodamine in solution resulted in predictable changes in fluorescence anisotropy (Supplemental Data, Supplemental Figure S3 available on *Cell* website; compare blue circles with theoretical curve in red). Similarly, considering that exogenously added C_6-NBD-SM in cell membranes is uni-

formly distributed in domains of very large size (with respect to the molecular size and R_0), we were able to precisely describe the changes in fluorescence anisotropy on increasing concentration of the fluorophore (Supplemental Data, Supplemental Figure S3 available on *Cell* website; compare blue circles with theoretical curve in red).

Thus, in the context of GPI-APs on the cell surface, reducing fluorophore concentration by photobleaching should have a predictable effect on anisotropy (see Supplemental Data, Supplemental Figure S1B available on *Cell* website); the exact profile will depend on how the fluorophores are organized relative to each other. We tested three spatial arrangements of GPI-APs (Figure 2A). Models **a** and **a'** represent domains where the size is much larger than molecular dimensions; this organization is most commonly portrayed in the literature as functional rafts (Edidin, 2001; Jacobson and Dietrich, 1999; Varma and Mayor, 1998). This picture is suggested by observation of phase-segregated domains in artificial membrane systems and from interpretations of DRM studies (Edidin, 2003). In Model **a** GPI-APs are uniformly distributed within domains of large radii ($\sim$10 times R_0, $\sim$50 nm) while in Model **a'** a fraction of the GPI-APs are organized as in Model **a**, while the remaining are dispersed as isolated fluorophores on the cell surface (Kenworthy and Edidin, 1998). Model **b** is merely an extension of the organization in Model **a** wherein GPI-APs are organized along the periphery of the raft. In all three cases, we impose the constraint that within domains, GPI-APs are densely clustered at distances less than R_0 ($\sim$0.9 R_0; see Table 1). We used FR-GPI labeled with PLF because it is readily photobleachable. The anisotropy of PLF-FR-GPI at the cell surface increases upon photobleaching, moving from 72% (0.178) to 85% (0.21) of A_∞ (0.247 $\pm$ 0.003; see Supplemental Data available on *Cell* website) after a reduction of 68% in intensity relative to the starting intensity, I_0 (Figures 2B and 2C; black symbols). This increase is different from that predicted in Models **a**, **a'**, and **b** (compare theoretical fits with data in Figures 2B and 2C); Model **a'**, fares better but the best-fit curve is still not in complete agreement with the experiment. (Additional data from hetero-FRET experiments [see below], rule out Model **a'**.) If Models **a** and **b** are force fit onto the data, while leaving the fluorophore density in each domain as a "fit" parameter, then the predicted fluorophore density in each domain is much lower (average intermolecular distance $\geq$2.5 R_0) than that obtained from the time-resolved anisotropy experiments (data not shown).

In searching for an alternative model, we note that the crucial features of the above models are that the size of the domain is much larger than R_0 and the molecular size and the density of proteins in the cluster is high. We thus consider a qualitatively different model, Model **c** (Figure 3A), wherein the size of the domain is comparable to R_0 and the molecular size. Figure 3B shows that the experimental data for PLF-FR-GPI is extremely well described by this model in which a fraction of molecules are in domains (when they undergo FRET) where the distance between any two molecules is not larger than R_0, while the remainder are dispersed as monomers on the cell surface. While we grant that the model that we consider may not be unique, we have

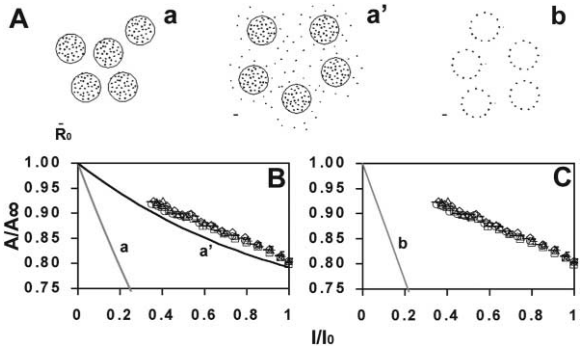

Figure 2. Photobleaching Induced Changes in Homo-FRET Rule Out Large-Sized Domains Containing GPI-APs

(A) Models of organization of GPI-AP's. Model **a**: GPI-APs are uniformly distributed within domains of radii $R \gg R_0 < l$ (l = molecular size). Model **a'**: A fraction of the GPI-AP's are organized as in Model **a**, while the remaining are dispersed as isolated fluorophores on the cell surface. Model **b**: GPI-APs are distributed uniformly on the periphery of domains of radii $R \gg R_0 < l$.

(B and C) Comparison of relative anisotropy profiles (A/A_∞) versus total intensity, I (relative to its value before photobleaching, I_0), calculated from Models **a** (B; gray line) and **a'** (B; black line) and **b** (C; gray line) using Forster's theory (Supplemental Data available on *Cell* website) with experimental anisotropy profiles (black symbols) determined from cells expressing different levels of GPI-AP obtained after photobleaching PLF-labeled FR-GPI. The profiles representing Models **a**, **a'** and **b** were calculated with parameters which best fit the entire data set while fixing the average intermolecular distance as 1.2 R_0 between fluorophores within domains for Models **a** and **b**, and 0.91 R_0 for Model **a'** with 30% of fluorophores in domains (for **a'**). Note Models **a**, **a'** or **b** fail to describe the experimental data.

considered all reasonable models of aggregation and are unable to find another configuration that can account for all the data. The qualitative feature of the change in anisotropy with the loss of fluorescence intensity in Figure 3B is contingent on (1) the existence of monomers and high-density clusters, and (ii) the size of the clusters being comparable to R_0 and the size of the molecule. The best fit to the data is obtained when we estimated the ratio of clusters to monomers by the method of least squares to be $\sim$22% (solid line in Figure 3B). Considering an acceptable range of parameters based on the lowest values of Δ (standard deviation; Figure 3C), and taking data across different cells (Figure 3D), we find that the fit provides a range of values for the fraction of GPI-APs present in clusters; 20%–40% of all GPI-AP species are engaged in FRET at any given time. Based on how many molecules of size 3 nm (for a 40 kDa FR-protein) can occupy a cluster of diameter R_0 ($\sim$5 nm), we get a rough upper bound of four molecules within the cluster.

We next studied the cluster to monomer distribution of GFP-GPI using a similar method. We find that the extent of change in anisotropy of GFP-GPI upon chemical quenching is consistent with Model **c** but for technical reasons (detailed in Supplemental Data available on *Cell* website) we prefer not to extract a value for the fraction of clusters and monomers. Instead, a lower bound ($\sim$10%; Table 1) on the cluster fraction may be obtained from the amplitude of the FRET component in the anisotropy decay experiments for both GFP-GPI and YFP-GPI. An upper bound may be obtained if we con-

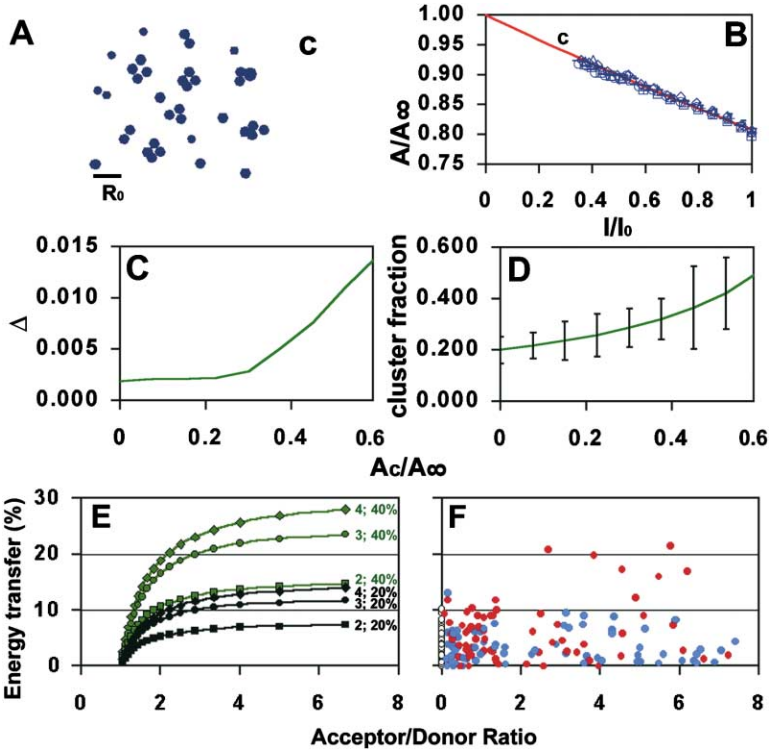

Figure 3. Photobleaching Induced Changes in Homo-FRET Show that GPI-APs Are Present as Monomers and Small Clusters, Consistent with Lack of Detectable Hetro-FRET

(A) Model **c**: GPI-APs are distributed as a collection of monomers (isolated proteins) and *n*-mers (with $n \geq 2$), with inter protein distances within an *n*-mer of the order of R_0, Forster's radius (scale bar).

(B) Comparison of experimental anisotropy profiles (symbols) determined from cells expressing different levels of GPI-AP obtained after photobleaching PLF-labeled FR-GPI with best-fit curve for Model **c** (red line). Fixing the steady-state anisotropy of an isolated fluorophore $A^{(1)} = A_\infty = 0.247$, and the steady state anisotropy of an *n*-mer, $A^{(2)} = A^{(3)} = A^{(4)} = 0.1\ A^{(1)} = A_C$, and $A^{(n)} = 0$ when $n \geq 5$, we find that 22% of fluorophores are present in clusters.

(C) Varying A_C, the steady state anisotropy of a cluster, we determine the best fit and the standard deviation Δ for the fraction of clusters amongst the anisotropy profiles of individual cells from a single dish. For values of $A_C/A_\infty < 0.35$, Model **c** shows a good fit with the data.

(D) Cluster fraction (line) at different values of A_C is the best fit to data collected over cells present in 10 different dishes. Vertical error bars correspond to the standard deviation in the cluster fraction. Given the optimum value of A_C/A_∞, we find that the range in the cluster fraction can be anywhere between 20%–40%.

(E) Efficiencies of energy transfer between donor (mCFP) and acceptor (mYFP) species versus different acceptor to donor ratios were calculated using Model c wherein the fluorophores appear as monomers and clusters of the indicated size *n*, as described in Supplemental Data available on *Cell* website. The values next to each curve indicate cluster size, *n*, and percentage of clusters used for determining the energy transfer efficiency.

(F) Energy transfer efficiency was measured on cells coexpressing different levels of mCFP-GPI and mYFP-GPI. The magnitude of hetero-FRET was determined by analyses of donor dequenching upon acceptor photobleaching in the absence (open circles) or presence of acceptor fluorophores (blue circles). Hetero-FRET was also measured on mCFP- and mYFP-GPI-expressing cells incubated with aerolysin toxin to increase the cluster size (red circles).

sider that after quantitative crosslinking of GFP with glutaraldehyde only ~30% of amplitude of the net anisotropy decay arises from the FRET (~0.3 ns; Table 1) component. Taking this value as the maximum amplitude from 100% of GFP species within R_0, ~30% of GFP-GPI molecules are likely to be present in high density clusters.

Although we detect robust homo-FRET between GPI-APs labeled with the same fluorophore, previous studies (Kenworthy and Edidin, 1998; Kenworthy et al., 2000) and our experiments using hetero-FRET to detect clustering between different GPI-AP species (GFP-GPI or FR-GPI, data not shown), or between two different GPI-APs (GFP-GPI and Alexa568-labeled anti-FR fab fragment against FR-GPI; mCFP-GPI and mYFP-GPI, Figure 3F) have failed to detect hetero-FRET beyond the level of noise in the system. As suggested by Kenworthy and Edidin, if 20% of the proteins were in large-sized clusters (as in Models **a**, **a'**, and **b**), hetero-FRET should have been detected even at low expression levels in the membrane (Kenworthy and Edidin, 1998).

Using two proteins, mCFP-GPI and mYFP-GPI, organized as described by Model **c**, we calculate the efficiency of hetero-FRET between these GPI-AP species for different donor and acceptor ratios (Figure 3E; see Supplemental Data available on *Cell* website for detailed methodology). The calculation takes into account: (1) the probability of finding a donor and acceptor in the same cluster, expectedly this factor considerably reduces the efficiency of FRET for small clusters; (2) the possibility of donor-donor transfer; and (3) values of homo and heterotransfer rates obtained from the spectral overlaps of the fluorophores and the experimentally determined densities in clusters. Predictably, we find that hetero-FRET efficiencies vary with donor acceptor ratios, cluster size, and the fraction of clusters and monomers (Figure 3E); large clusters give rise to more hetero-FRET, at similar cluster to monomer and donor acceptor ratios. Considering that we were unable to detect hetero-FRET beyond the threshold variation inherent in such an experiment (± 12%; Figure 3F, compare open with blue circles), this clearly limits the size of GPI-APs clusters (<4 molecules) and/or low cluster to monomer ratios (~20%). To ensure that our setup is indeed capable of detecting the presence of larger sized clusters of GPI-APs when they are present in cell membranes, we have used the heptamerizing aerolysin toxin (Y221G mutant), which binds GPI-APs via the GPI-anchor (Fivaz et al., 2002). As shown in Figure 3F (red circles), aerolysin toxin Y221G induces significant and detectable hetero-FRET for the same acceptor to donor ratios.

Taken together, the absence of detectable hetero-

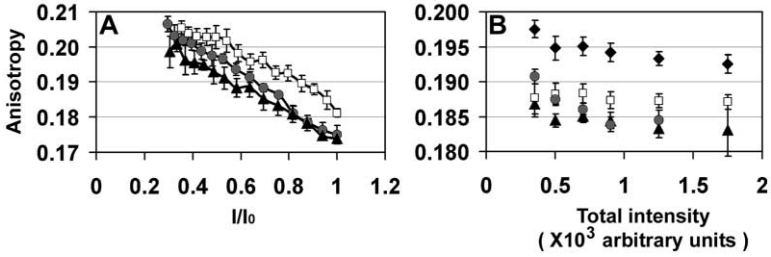

Figure 4. Effects of Cholesterol and Sphingolipid Depletion on GPI-AP Organization

(A) Steady-state anisotropy values from PLF-labeled-FR-GPI in untreated (black triangles), sphingolipid-depleted (gray circles), or cholesterol-depleted cells (open squares) plotted against normalized intensities (I/I_0) of individual cells obtained after different photobleaching times as described in Figure 2. The data were fit to parameters (A_c/A_∞) and show that the fraction of monomers and clusters in sphingolipid-depleted cells is unchanged with respect to control cells (20%–40%) while it is significantly reduced (10%–20%) in cholesterol-depleted cells.

(B) Anisotropy versus intensity profiles of PLF-FR-GPI in LYB cells either undepleted (black triangles), depleted of cholesterol by treatment with cyclodextrin (1 mM, 30 min; open squares), extensively depleted of sphingolipid (gray circles), or depleted of both cholesterol and sphingolipid (black diamonds), indicate that sphingolipid depletion augments the ability of cyclodextrin to alter the organization of GPI-APs. Mean and standard error from the mean of each data point were obtained from two dishes each with at least 130 cells. Similar data were obtained in two different experiments.

FRET and the presence of robust homo-FRET consistent with a minor fraction (~20%–40%) of small (≤ 4) dense GPI-AP aggregates; the remaining proteins must exist as monomers for all the different GPI-AP species examined.

Cholesterol and Sphingolipid Depletion Differentially Affect GPI-AP Clustering

Depletion of cholesterol from CHO cells expressing either FR-GPI (Varma and Mayor, 1998) or GFP-GPI by treating cells with the cholesterol lowering agents, compactin, methyl-β-cyclodextrin (data not shown), or saponin results in a loss of homo-FRET (i.e., the fast component of anisotropy decay) between GFP-GPI species and between mYFP-GPI compared to the corresponding values for undepleted cells (Table 1). Following treatment with compactin, the change in anisotropy upon fluorophore photobleaching clearly shows a different profile from untreated cells (Figure 4A, compare black triangles with red open squares, for untreated and treated cells, respectively). As calculated from Model **c** (Supplemental Data available on *Cell* website), these data are still consistent with the presence of a mixture of clusters and monomers, but with a reduced cluster-to-monomer ratio (from 20%–40% to 10%–20%). This provides evidence that the nanometer scale organization of GPI-APs is mediated by cholesterol levels in the membrane.

On the other hand, in cells depleted of sphingolipids to levels that relieve endocytic retention either by treatment with a sphingolipid synthesis inhibitor, Fumonisin B_1 (data not shown) or in a sphingolipid auxotroph grown under sphingolipid deficient conditions (Chatterjee et al., 2001), the anisotropy value of FR-GPI and the cluster to monomer ratios at the cell surface remain unchanged (Figure 4A; compare black triangles with gray circles, for control and sphingolipid-depleted cells, respectively). Similar results were obtained with GFP-GPI (data not shown). This suggests that sphingolipids do not play an irreplaceable role in the organization of the nanoscale clusters. However, after sphingolipid depletion, while cholesterol is easily extracted from the cells membranes by cyclodextrin (Fukasawa et al., 2000), FR-GPI clusters also become more sensitive to cholesterol extraction compared to undepleted cells; PLF-FR-GPI exhibits higher steady state anisotropy values in double-depleted cells (Figure 4B; compare black triangles and open squares with black diamonds for the double-depleted cells). These observations show that sphingolipid levels influence the availability of cholesterol for stabilizing the GPI-AP clusters at the cell surface, consistent with an indirect role for sphingolipids in the formation of these nanoscale clusters.

Multiple GPI-APs Inhabit the Same Nanometer-Sized Cluster

We now ask whether a potential consequence of the ability of the GPI-anchor to induce a nanometer-sized clustered distribution is to promote the coexistence of multiple GPI-APs in a single cluster (Figure 5A). Consistent with the small size of the cluster, we do not detect any hetero-FRET between two different GPI-APs at different donor and acceptor densities (Figure 3F). Thus, one way to look for the cohabitation of two proteins in the same cluster would be to monitor the extent of homo-FRET exhibited by a labeled GPI-APs by the expression of a potentially interacting protein present in the same cluster (Figure 5A). We find that the anisotropy of GFP-GPI increases with an increase in the ratio of the expression level of FR-GPI to GFP-GPI (Figure 5B; black diamonds). In contrast, the anisotropy of GFP-GPI is independent of similar expression levels of a transmembrane-anchored FR isoform (Figure 5B; open squares). Conversely, the anisotropy of GFP-PIT is independent of the expression of FR-GPI in the same membrane (data not shown). This interaction is not specific to a single GPI-AP pair, since PLF-FR-GPI (Figure 6B; black circles) and GFP-GPI (Figure 6C; black diamonds) also exhibit similar shifts in anisotropy when another GPI-AP, decay accelerating factor (DAF), is coexpressed in the same membrane. An important feature of the increase in anisotropy observed with the coexpression of a second GPI-AP is that it is related to the ratio of the two proteins in the membranes and not to the individual densities of the proteins in the membrane. A given value of ratio results from a range of expression levels of both proteins (Supplemental Data, Supplemental Figure S4 available on *Cell* website), ruling out the possibility that the combined expression of two GPI-APs depletes a critical limiting component, for example, cholesterol, for

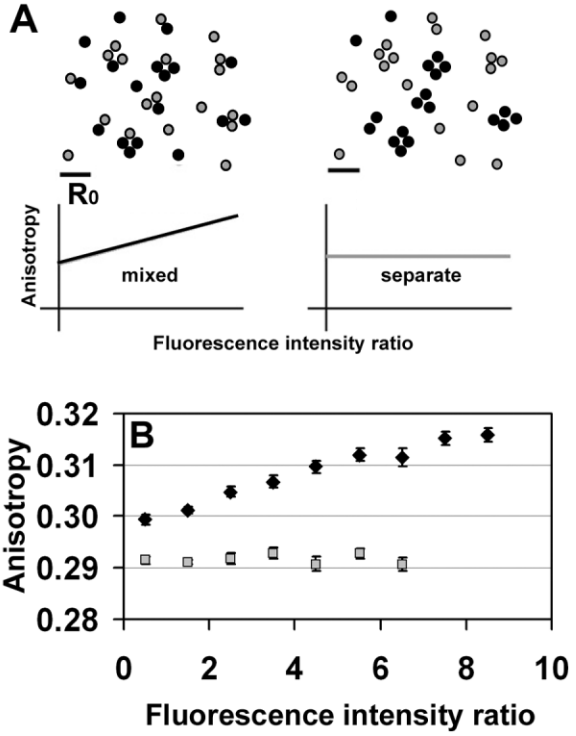

Figure 5. Multiple GPI-APs Are Present in the Same Cluster

(A) In the schematic, if two different GPI-APs (gray and black circles) occupy the same cluster (left), increasing expression of one GPI-AP (black circles) will lead to decreasing number of homo-FRET events. As a result, homo-FRET between gray circles species will decrease. Consequently, there will be an increase in emission anisotropy of the fluorescent GPI-AP species being monitored. Alternatively, if different GPI-AP species are present in separate clusters (right), there will be no change in the anisotropy of the fluorescent species being monitored with increased expression of one of the proteins. cDNAs encoding GFP-GPI (B) was transiently transfected into FR-isoform (FR-GPI, black diamonds; FR-TM, open squares)-expressing cells and the fluorescence intensities of Cy5-conjugated Fab fragment of monoclonal antibody Mov19 (Cy5-anti-FR-Fab) and GFP were measured to determine the expression levels of the individual proteins and emission anisotropy of GFP-GPI, respectively. Mean values of anisotropy (± SE) were determined for ratio ranges (± 0.5), and plotted against the midpoint of the corresponding ratio ranges of Cy5-labeled anti-FR-Fab to GFP-GPI.

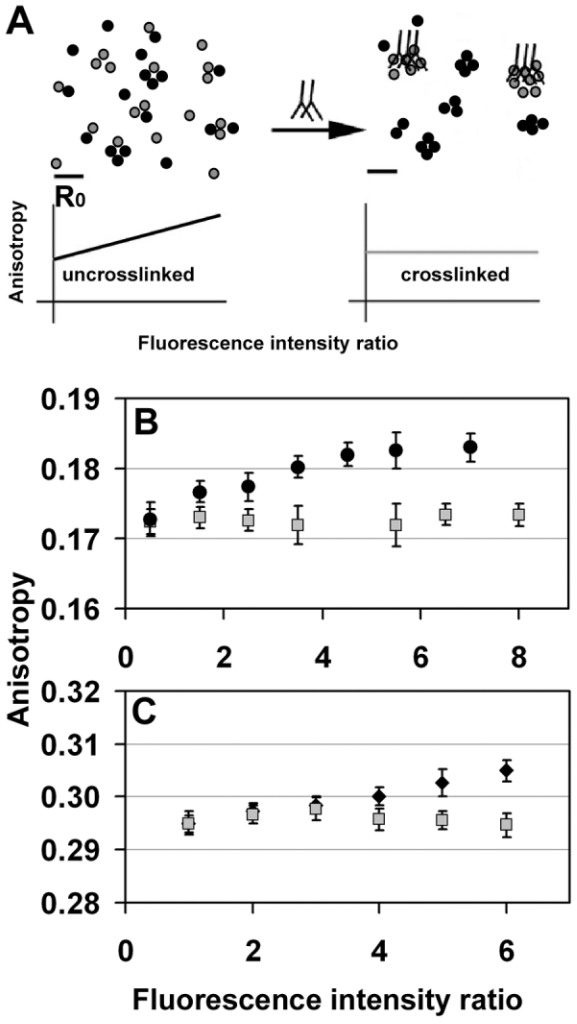

Figure 6. Antibody Mediated Crosslinking Reorganizes Native GPI-APs Clusters

(A) Schematic showing the effect of crosslinking of one GPI-AP species (gray circles) on emission anisotropy of the noncrosslinked species (black circles). If the noncrosslinked species is reorganized, the dependence of anisotropy on the expression level of the other (crosslinked) species is lost. cDNAs encoding FR-GPI (B) and GFP-GPI (C) were transfected into DAF-expressing cells. The fluorescence intensities of Cy5-conjugated Fab fragment of monoclonal antibody IA10 (Cy5-anti-DAF), PLF-FR-GPI (B), and GFP (C) were measured to determine the expression levels of the individual proteins. Fluorescence intensities and corresponding emission anisotropy of PLF-labeled FR-GPI (B) and GFP-GPI (C) were determined before (black circles and diamonds, respectively) and after (open squares) antibody-mediated crosslinking of DAF. Mean values of anisotropy (± S.E.) were determined for ratio ranges (± 0.5), and plotted against the midpoint of the corresponding ratio ranges of anti-DAF (B and C) to PLF-FR-GPI (B) or GFP-GPI (C) intensities as indicated.

the first protein. These results provide evidence that more than one protein-species inhabits a single cluster solely due to attachment to the membrane by a GPI-anchor.

Antibody-Crosslinking Reorganizes Preexisting Clusters and Alters Endocytic Routing of Crosslinked Proteins

Antibody-mediated crosslinking reorganizes a specific GPI-AP (for example, DAF) into visible and stable clusters (Mayor and Maxfield, 1995), but it does not visibly alter the diffuse distribution of other coexpressed GPI-APs (for example, GFP-GPI or PLF-FR-GPI; Supplemental Data, Supplemental Figure S5 available on *Cell* website; see also Mayor et al., 1994) expressed in the same membrane. To examine whether crosslinking of a specific GPI-AP (DAF) reorganizes the noncrosslinked species at the level of the nanometer scale clusters we monitored anisotropy of GFP-GPI and PLF-FR-GPI after crosslinking coexpressed DAF. The anisotropy values of GFP-GPI and PLF-FR-GPI are restored to the values observed in the absence of DAF expression (Figures 6B and 6C) after crosslinking DAF. Similar data have been obtained in the case of the GFP-GPI and FR-GPI pair;

crosslinking FR-GPI restores the anisotropy of GFP-GPI to the valve observed in the absence of FR-GPI (data not shown). These results suggest that the crosslinked species is removed from the preexisting clusters, and in the process the composition of the preexisting clusters is reorganized (Figure 6A).

We next investigated the effect of antibody-mediated crosslinking on endocytic trafficking of GPI-APs. We have recently reported that GPI-anchoring specifies internalization via a dynamin-independent endocytic pathway into GPI-AP-enriched endocytic compartments (GEECs). This pathway is also responsible for a major fraction of the fluid-phase uptake (Sabharanjak et al., 2002). Here, we examined the endocytic route of the crosslinked and noncrosslinked GPI-AP's. Native, noncrosslinked GPI-APs are endocytosed via GEECs (Figures 7A–7D) into recycling compartments, however, if FR-GPIs are crosslinked by primary and secondary antibodies into small visible clusters and allowed to be endocytosed for up to one hour, the internalized crosslinked structures do not reach the recycling compartment (Supplemental Data, Supplemental Figure S6 available on *Cell* website). At an early time after endocytosis, crosslinked complexes are excluded from FITC-dextran-containing GEECs (Figures 7E–7H). Instead, they are predominantly found in transferrin-containing endosomes (Figures 7I–7L) implying that they are endocytosed via the clathrin-mediated pathway; thus, the size of the crosslinked cluster is not an impediment to endocytosis per se. In cells expressing both FR-GPI and GFP-GPI, if FR-GPI was extensively crosslinked with antibodies, its endocytosis was prevented, however, noncrosslinked GFP-GPI continues to be internalized normally via the GEEC route (Supplemental Data, Supplemental Figure S7 available on *Cell* website). These data show that antibody crosslinking segregates the protein from the preexisting clusters, and simultaneously alters endocytic sorting of the GPI-AP at the cell surface and its endocytic fate. This suggests that association with preexisting nanoscale clusters determines the specific endocytic route and destination for GPI-APs.

Discussion

The Size and Composition of GPI-AP-Associated Structures at the Surface of Living Cells

To investigate the functional architecture of rafts on the plasma membrane, we have studied the spatial distribution of one of the constituents and examined functional consequences of perturbation of this organization. We have provided evidence that a small but significant fraction of GPI-APs form extremely high density clusters of nanometer size ($\sim$4–5 nm), each consisting of a few ($\leq$4) molecules and different GPI-AP-species.

The high local density of GPI-AP molecules is directly derived from the FRET-related fast anisotropy decay rates observed in time-resolved anisotropy measurements, with an interprotein distance less than 4 nm in the cluster. The amplitude of the component corresponding to the fast decay rate indicates that not less than 10% of the GPI-AP species are present in clusters. Additionally, both the nanometer-size and fraction of clusters are obtained from two independent types of experiments. First, fluorescence photobleaching experiments and theoretical modeling of resultant changes in anisotropy, in conjunction with a knowledge of the interprotein distances shows that 20%–40% of GPI-AP species are present in clusters on the scale of R_0, (i.e., $<$4.65 nm). Second, the lack of detectable hetero-FRET between identical and dissimilar GPI-AP species (Kenworthy and Edidin, 1998; Kenworthy et al., 2000) while observing relatively robust homo-FRET can be explained by the presence of a fraction ($<$30%) of small clusters ($<$3–4 molecules in number) in the presence of a large monomer pool. Our results also suggest that multiple species of GPI-Aps, but not transmembrane isoforms of the same proteins, inhabit the same nanocluster.

These results are also consistent with recent single fluorophore tracking studies conducted on a GPI-anchored isoform of class II MHC molecules (Vrljic et al., 2002) which reported fast Brownian diffusion motion of almost all molecules and only a small fraction (between 6 and 20%) of the labeled species with a significantly slower diffusion coefficient consistent with larger oligomers. However these studies were unable to characterize the size or origin of the slowly diffusing species.

Concentration Independent Anisotropy, Cluster Distribution, and Large-Scale Organization

To understand the mechanism of clustering of GPI-APs, we perturb this organization by a variety of means. Cholesterol depletion or replacement of the GPI-anchor with a transmembrane domain abrogate association with the nanoscale clusters indicating that the roles of cholesterol and the GPI-anchor are central to the formation of GPI-AP nanoclusters; cohabitation of multiple GPI-APs in the same nanocluster provides additional evidence that they are formed by lipid-based mechanisms. Perturbation of this organization by antibody crosslinking suggests that interactions holding the GPI-AP species together are likely to be weak; over short length scales antibody crosslinked proteins can be induced to detach and reorganize into distinct structures.

Any mechanism for the formation of the GPI-AP clusters must be consistent with the following features: (1) the capacity of the clusters to undergo exchange (as observed during crosslinking) and (2) the observed concentration independence of the steady state anisotropy over a large range of expression levels, implying a fixed proportion of monomers and clusters over this concentration range. This brings out an apparent contradiction; dynamic exchange would result in a distribution of monomers and clusters consistent with chemical equilibrium and inconsistent with the existence of fixed proportion of monomers and clusters (see Supplemental Data available on *Cell* website for theoretical explanation). This contradiction may be resolved if clusters are formed in actively generated "domains" that do not allow for ready mixing. This would suggest that the monomer and cluster distribution is likely to be determined by active processes. The ability of cholesterol levels to modulate the fraction of clusters and monomers suggests that cholesterol homeostasis in turn regulates this activity. Although reduction in sphingolipid levels has no direct effect on the relative concentration of nanoscale clus-

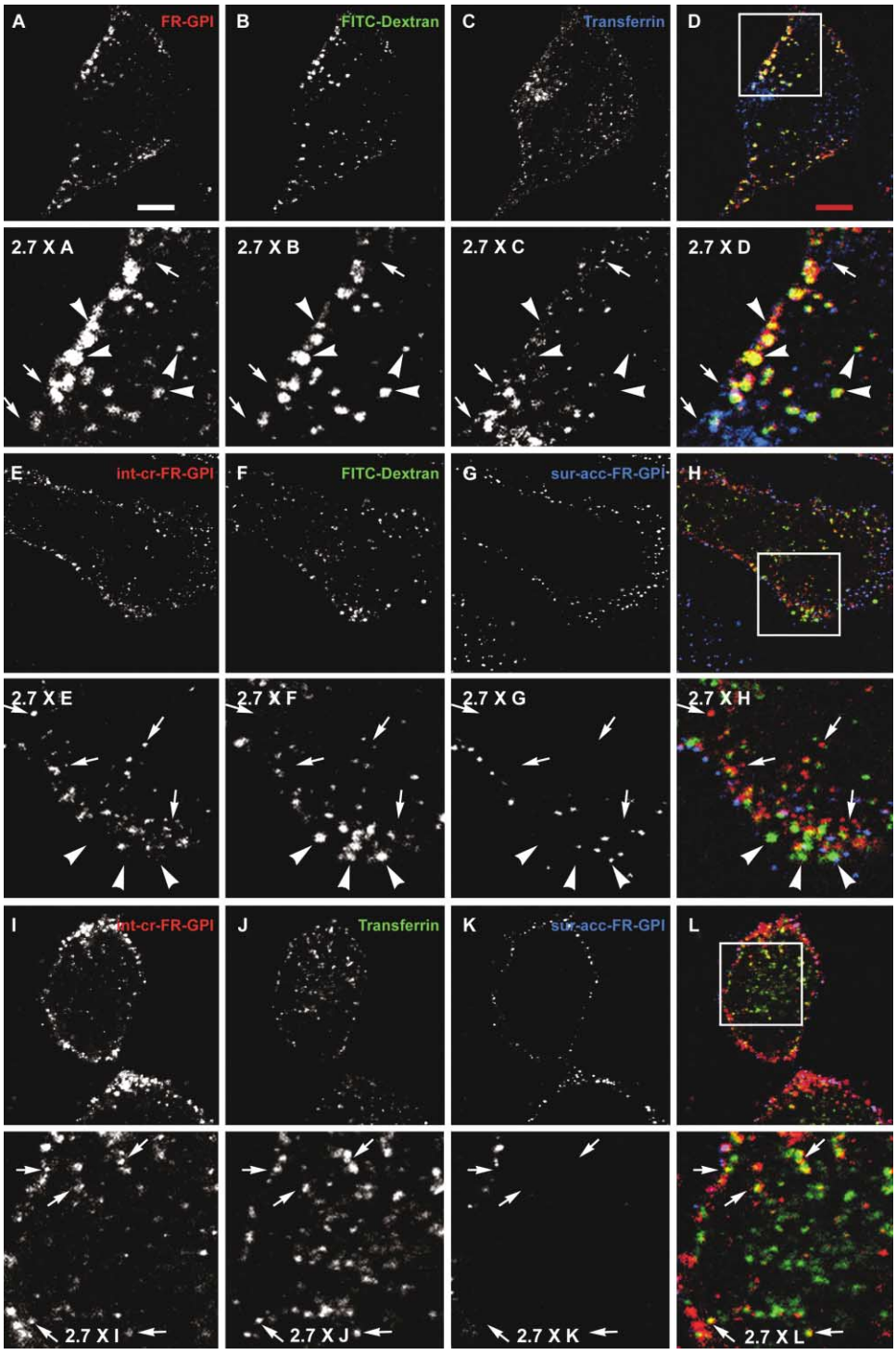

Figure 7. Antibody-Crosslinked GPI-APs Are Excluded from the Native GPI-AP-Specific Endocytic Pathway in CHO Cells

(A–D) Cy3-labeled anti-FR Fab (Mov18) fragment against FR-GPI (A, red in D), FITC-dextran (B, green in D) and Cy5-labeled transferrin (C, blue in D) were cointernalized in FR-GPI-expressing CHO cells for 5 min at 37°C.

(E–L) Mouse monoclonal, Mov18, bound to FR-GPI was crosslinked with a Cy5-labeled secondary antibody (E, red in H), or Alexa568-labeled secondary antibody (I, red in L) into small clusters by incubation for 30 min on ice. Cells were the incubated with FITC-Dextran (F, green in H), or Cy5-labeled transferrin (J, green in L) for 5 min at 37°C. Endosomes containing internalized crosslinked FR-GPI were identified as surface-inaccessible structures that do not counterstain with appropriately-labeled tertiary antibodies (G, and K, blue in H, and L) added on ice. Boxed areas in the images of internalized probes obtained from a single confocal plane are shown at higher magnification in the panels immediately below. Most of the endocytosed noncrosslinked FR-GPI is present in FITC-dextran-filled GEECs (arrowheads; A–D), distinct from transferrin-containing endosomes (arrows; A–D). After crosslinking and endocytosis, internalized FR-GPI (int-cr-FR-GPI) is clearly distinguished from the spatially segregated surface-accessible crosslinked FR-GPIs (sur-acc-FR-GPI; G, K: blue in H and L) at the cell periphery. Note that internalized crosslinked FR-GPI endosomes do not colocalize with FITC-dextran-containing GEECs (E–H; arrowheads), instead are mainly found colocalized with internalized transferrin (I–L; arrows). Scale bar is equal to 10 μm.

ters, the enhanced susceptibility of these clusters to cholesterol-depletion at the cell surface in sphingolipid-depleted cells suggests that both cholesterol and sphingolipids are involved in this higher level organization. In sphingolipid-depleted cells, other lipids such as phosphatidylcholine may substitute, albeit poorly for the functions of sphingolipids. Additional experiments are necessary to address the active nature and the spatiotemporal scales of this higher level organization.

Our observations show that "preexisting" structures of GPI-APs at the surface of living cells undergo significant reorganization upon crosslinking; the nanoscale clusters are reconfigured and larger and longer-lived crosslinked structures are induced with different consequences for endocytosis and signaling. However, both the crosslinked and noncrosslinked GPI-APs are quantitatively associated with DRMs (P.S. and S.M., unpublished data), once again indicating that DRM-association is too coarse and provides little structural and functional insight. Thus, the FRET-methodology described here will have to be routinely adapted to study lipid-dependent raft organization, due to its nonperturbing nature, sensitivity, and nanometer resolution.

Functional Consequences of Nanoscale Clustering

A combination of monomers and small clusters represent a compromise between enhanced binding affinities and dynamic range of sensitivities (Bray et al., 1998; Irvine et al., 2002). Since the cluster/monomers distribution is likely to be determined by an active mechanism in the cell, this suggests that the response behavior of cells will depend on the state of the cell (e.g., cholesterol homeostasis), thereby contributing to the diversification of cellular responses. Nanoscale-clustering also provides a natural explanation for the ability of low concentrations of ligands to efficiently bind GPI-anchored receptors (e.g., heparin sulfate proteoglycans, folate receptors, and cell adhesion molecules), with functional consequences at least in the context of folate transport (Matsue et al., 1992) and integrin function (Carman and Springer, 2003). The presence of multiple GPI-AP species in a tight cluster has potential for tuning the specificity of cell-cell adhesion function since many adhesion molecules are GPI-anchored (Harris and Siu, 2002). More significantly, this nanoscale clustering could be utilized in the conversion of GPI-anchored prion proteins to infectious scrapie (Kaneko et al., 1997; Taraboulos et al., 1995). These clusters would also provide a high density of prion molecules in the plane of the membrane required for efficient conversion to the scrapie form with monomers providing a constant source of substrate for the transconfiguration.

As we have demonstrated earlier, GPI-anchoring appears to be necessary for targeting proteins to a specific dynamin-independent, cdc42-regulated endocytic pathway (Sabharanjak et al., 2002; Sharma et al., 2002). Crosslinking alters the ability of GPI-APs to associate with the preexisting clusters and prevents endocytosis via GEECs but not via the clathrin-dependent pathway. Although other explanations are possible, these results indicate that the organization of GPI-APs into nanoscale clusters serves as a sorting signal for specific endocytic routing. This is further substantiated by the observation that any attempt to convert the GPI-APs to monomers by cholesterol depletion (R. Chadda, M. Kalia, S. Sabharanjak, S. Chatterjee, M.R., and S.M., unpublished data), or exchanging the GPI-anchor with a transmembrane anchor as in the case of FR-GPI and GFP-GPI (Sabharanjak et al., 2002), prevents endocytosis via the GEEC pathway. We propose that the nanoscale clusters associated with a potentially actively maintained sphingolipid, cholesterol-dependent domain, define an endocytically active zone.

Conclusion

Our results show that GPI-anchoring provides a mechanism for bringing diverse proteins within nanometer proximity of each other in small clusters. At a functional level, the preexisting organization that we have discovered has implications for sorting and the (patho)physiology of many GPI-APs, while the "induced structures" may be crucial for signal transduction or sorting. The observations presented here suggest a hierarchical picture of an active lipid-dependent organization at different length scales that are exploited for distinct functions.

Experimental Procedures

Theoretical Analyses

All theoretical modeling and analyses are available as Supplemental Data on the *Cell* website.

Cell Culture, Antibodies, and Labeling Protocols

Cell culture, antibodies, fluorescent probes including GFP-GPI, mCFP, and mYFP-GPI (derived from EGFP variants where nomenclature for GFP variants follow Tsien, 1998), and labeling protocols are as described previously (Sabharanjak et al., 2002; Varma and Mayor, 1998) unless otherwise specified in Supplemental Data available on *Cell* website.

Steady-State and Time-Resolved Anisotropy Measurements

Measurements of fluorescence emission anisotropy of labeled proteins in living cells were carried out essentially as described (Varma and Mayor, 1998) with the modifications described in Supplemental Data (available on *Cell* website). Time-resolved anisotropy measurements were made on a Nikon Diaphot 300 microscope fitted with a 20 $\times$ 0.75 NA objective maintained at room temperature, using a TCSPC setup and analyzed as previously described (Lakshmikanth and Krishnamoorthy, 1999) with modifications in the analysis procedures as described in Supplemental Data (available on *Cell* website).

Acceptor Photobleaching Hetero-FRET

Acceptor photobleaching hetero-FRET experiments were carried out on a Bio-Rad MRC1024 laser scanning confocal microscope (GFP-Alexa568 and Alexa568-Cy5 pairs) or a wide field microscope (mCFP-mYFP pair) equipped with appropriate filter sets as described earlier (Krishnan et al., 2001). GPI-AP expressing cells were labeled with donor (Alexa568) and acceptor fluorophores (Cy5) labeled Fab fragments of specific antibodies (Mov18 against FR-GPI and 1B3A8 against GFP (Sabharanjak et al., 2002) at fixed ratios of 1:1 and 1:3. Efficient (>60%) hetero-FRET efficiency (defined as)

$$E\% = \left[1 - \frac{Donor_{pre}}{Donor_{post}}\right] \times 100$$

is detected between Alexa568 and Cy5-labeled Fab fragments of Mov18 and Mov19, respectively which bind noncompetitively to the same FR-GPI protein, confirming that these fluorophores and the method are capable of reporting a FRET signal. For the mCFP and mYFP pair, the mCFP signal was corrected for photobleaching ($\leq$ 10%), prior to calculating the FRET efficiency as above. The extent of mCFP photobleaching was determined in the absence

of the mYFP acceptor under the same experimental conditions. Heptamer forming GPI-anchor binding toxin, aerolysin (Y221G; Fivaz et al., 2002), was used at a concentration between 0.5 and 1 μg/ml, to induce large-sized clusters.

Image Analysis

All image processing and analyses were done using Metamorph software (Universal Imaging, PA) and Microsoft Excel as described (Varma and Mayor, 1998) with modifications listed in Supplemental Data available on *Cell* website.

Interactions between Multiple GPI-APs and Antibody-Mediated Crosslinking

For probing interactions between multiple proteins, fluorescence intensity of the interacting species was measured by imaging cells labeled with Cy5-conjugated antibodies against the protein in question. For this purpose, we transfected GFP-GPI into CHO cells expressing either FR-GPI, or the transmembrane anchored FR-isoform, alternatively GFP-GPI or FR-GPI were transfected into cells expressing another GPI-AP, DAF. Antibody-mediated crosslinking was performed as described earlier (Mayor and Maxfield, 1995). The ratio of intensities of Cy5-fluorescence to PLF (in FR-GPI expressing cells) or GFP fluorescence for individual cells was recorded along with the corresponding anisotropy values of PLF or GFP. To compare relative levels of the interacting protein in the same experiment, fluorescence intensity of cells labeled with the crosslinking secondary antibody was normalized to the maximum fluorescence value obtained from cells labeled with Cy5-labeled Fab fragment. Anisotropy values of individual cells were grouped into suitable intensity or ratio intervals as indicated. Weighted mean and standard error from duplicate dishes were obtained by considering the average anisotropy, and standard deviation for each interval as described. Pseudocolored total intensity and anisotropy images of cells were obtained as described earlier (Varma and Mayor, 1998).

Endocytic uptake experiments and confocal imaging were carried out essentially as described earlier (Sabharanjak et al., 2002). In the experiments where small clusters of GPI-APs were generated, labeled secondary antibodies (goat antimouse polyclonal antibodies; Jackson Laboratories) were incubated for 30 min on ice with cells preincubated with unlabeled primary mouse monoclonals against the respective GPI-AP. After endocytic uptake at 37°C for the indicated times, cells were treated with PI-PLC for 30 min on ice. Internalized, PI-PLC-resistant, crosslinked proteins were identified by colocalization with cointernalized probes and their inability to bind appropriately fluorescently labeled antigoat polyclonal antibody at the cell surface (sequentially applied on ice for 1 hr).

Determination of R_0 and Distance between Fluorophores

The Forster's radius R_0 was determined exactly as described (Lakowicz, 1999), using the formula: $R_0 = (8.8 \times 10^{23}\ \kappa^2\eta^{-4}Q_D J)^{1/6}$(Å) where, κ, the orientation factor was taken as 2/3, the refractive index $\eta = 1.4$, and $Q_D = 0.4$; the overlap integrals, $J = 3.52 \times 10^{-13}$ (Alexa568-Alexa568), 2.39×10^{-12} (Alexa568-Cy5) $M^{-1}cm^3$ were determined analytically. The rates of decay of fluorescence anisotropy due to FRET processes were utilized to determine the distances between fluorophores using procedures described previously (Gautier et al., 2001; Tanaka and Mataga, 1979). Interfluorophore distances R^R, were calculated considering R_0 and that the anisotropy decay times,

$$\tau_{r1} = \frac{1}{2\omega}$$

where

$$\omega = \frac{3}{2}\kappa^2 \left(\frac{R_0}{R}\right)^6 \tau_F^{-1},$$

τ_F = average fluorescence lifetime and $\kappa^2 = 2/3$. Standard deviations in estimating R were obtained by the method of propagation of errors.

Acknowledgments

This work was in part supported by a Senior Research Fellowship from The Wellcome Trust (grant # 056727/Z/99, S.M.); the National Centre for Biological Sciences; and a Swarnajayanthi grant from DST, India (M.R.). P.S. and R.V. are recipients of the Kanwal Rekhi fellowship from the TIFR Endowment Fund. We are grateful to M Edidin for making available the GFP-variants, and along with M.K. Mathew, K.S. Krishnan, and F.J. Barrantes for providing insightful comments, G. Gupta and A. Sarin for providing critical comments on the manuscript. We wish to thank B. Rami for help with the DLS experiments, N. Vyas for help with molecular biology, and Shafat Ahmad for purifying GFP. S.M thanks F.F. Bosphorus and K. Belur for inspiration.

Received: March 5, 2003
Revised: January 26, 2004
Accepted: February 2, 2004
Published: February 19, 2004

References

Agranovich, V.M., and Galanin, M.D. (1982). Electronic Excitation Energy Transfer in Condensed Matter (Amsterdam: North Holland Publishing Co.).

Anderson, R.G., and Jacobson, K. (2002). A role for lipid shells in targeting proteins to caveolae, rafts, and other lipid domains. Science *296*, 1821–1825.

Bray, D., Levin, M.D., and Morton-Firth, C.J. (1998). Receptor clustering as a cellular mechanism to control sensitivity. Nature *393*, 85–88.

Brown, D.A., and London, E. (2000). Structure and function of sphingolipid- and cholesterol-rich membrane rafts. J. Biol. Chem. *275*, 17221–17224.

Carman, C.V., and Springer, T.A. (2003). Integrin avidity regulation: are changes in affinity and conformation underemphasized? Curr. Opin. Cell Biol. *15*, 547–556.

Chatterjee, S., and Mayor, S. (2001). The GPI-anchor and protein sorting. Cell. Mol. Life Sci. *58*, 1969–1987.

Chatterjee, S., Smith, E.R., Hanada, K., Stevens, V.L., and Mayor, S. (2001). GPI anchoring leads to sphingolipid-dependent retention of endocytosed proteins in the recycling endosomal compartment. EMBO J. *20*, 1583–1592.

Clayton, A.H., Hanley, Q.S., Arndt-Jovin, D.J., Subramaniam, V., and Jovin, T.M. (2002). Dynamic fluorescence anisotropy imaging microscopy in the frequency domain (rFLIM). Biophys. J. *83*, 1631–1649.

Edidin, M. (2001). Shrinking patches and slippery rafts: scales of domains in the plasma membrane. Trends Cell Biol. *11*, 492–496.

Edidin, M. (2003). The state of lipid rafts: from model membranes to cells. Annu. Rev. Biophys. Biomol. Struct. *32*, 257–283.

Fivaz, M., Vilbois, F., Thurnheer, S., Pasquali, C., Abrami, L., Bickel, P.E., Parton, R.G., and van der Goot, F.G. (2002). Differential sorting and fate of endocytosed GPI-anchored proteins. EMBO J. *21*, 3989–4000.

Friedrichson, T., and Kurzchalia, T.V. (1998). Microdomains of GPI-anchored proteins in living cells revealed by crosslinking. Nature *394*, 802–805.

Fukasawa, M., Nishijima, M., Itabe, H., Takano, T., and Hanada, K. (2000). Reduction of sphingomyelin level without accumulation of ceramide in Chinese hamster ovary cells affects detergent-resistant membrane domains and enhances cellular cholesterol efflux to methyl-beta-cyclodextrin. J. Biol. Chem. *275*, 34028–34034.

Gautier, I., Tramier, M., Durieux, C., Coppey, J., Pansu, R.B., Nicolas, J.C., Kemnitz, K., and Coppey-Moisan, M. (2001). Homo-FRET microscopy in living cells to measure monomer-dimer transition of GFT-tagged proteins. Biophys. J. *80*, 3000–3008.

Hao, M., Mukherjee, S., and Maxfield, F.R. (2001). Cholesterol depletion induces large scale domain segregation in living cell membranes. Proc. Natl. Acad. Sci. USA *98*, 13072–13077.

Harris, T.J., and Siu, C.H. (2002). Reciprocal raft-receptor interactions and the assembly of adhesion complexes. Bioessays *24*, 996–1003.

Heerklotz, H. (2002). Triton promotes domain formation in lipid raft mixtures. Biophys. J. *83*, 1–7.

Heerklotz, H., Szadkowska, H., Anderson, T., and Seelig, J. (2003). The sensitivity of lipid domains to small perturbations demonstrated by the effect of triton. J. Mol. Biol. *329*, 793–799.

Irvine, D.J., Hue, K.A., Mayes, A.M., and Griffith, L.G. (2002). Simulations of cell-surface integrin binding to nanoscale-clustered adhesion ligands. Biophys. J. *82*, 120–132.

Jacobson, K., and Dietrich, C. (1999). Looking at lipid rafts? Trends Cell Biol. *9*, 87–91.

Kaneko, K., Vey, M., Scott, M., Pilkuhn, S., Cohen, F.E., and Prusiner, S.B. (1997). COOH-terminal sequence of the cellular prion protein directs subcellular trafficking and controls conversion into the scrapie isoform. Proc. Natl. Acad. Sci. USA *94*, 2333–2338.

Kenworthy, A.K., and Edidin, M. (1998). Distribution of a glycosylphosphatidylinositol-anchored protein at the apical surface of MDCK cells examined at a resolution of 100 A using imaging fluorescence resonance energy transfer. J. Cell Biol. *142*, 69–84.

Kenworthy, A.K., Petranova, N., and Edidin, M. (2000). High-resolution FRET microscopy of cholera toxin B-subunit and GPI-anchored proteins in cell plasma membranes. Mol. Biol. Cell *11*, 1645–1655.

Krishnan, R.V., Varma, R., and Mayor, S. (2001). Fluorescence methods to probe nanometer-scale organization of molecules in living cell membranes. J. Fluorescence *11*, 211–226.

Lakowicz, J.R. (1999). Principles of fluorescence spectroscopy, 2nd ed. (New York: Kluwer Academic/Plenum Publishers).

Lakshmikanth, G.S., and Krishnamoorthy, G. (1999). Solvent-exposed tryptophans probe the dynamics at protein surfaces. Biophys. J. *77*, 1100–1106.

Matsue, H., Rothberg, K.G., Takashima, A., Kamen, B.A., Anderson, R.G., and Lacey, S.W. (1992). Folate receptor allows cells to grow in low concentrations of 5-methyltetrahydrofolate. Proc. Natl. Acad. Sci. USA *89*, 6006–6009.

Mayor, S., and Maxfield, F.R. (1995). Insolubility and redistribution of GPI-anchored proteins at the cell surface after detergent treatment. Mol. Biol. Cell *6*, 929–944.

Mayor, S., and Riezman, H. (2004). Sorting GPI-anchored proteins. Nat. Rev. Mol. Cell Biol. *201*, 110–120.

Mayor, S., Rothberg, K.G., and Maxfield, F.R. (1994). Sequestration of GPI-anchored proteins in caveolae triggered by cross-linking. Science *264*, 1948–1951.

Parton, R.G., Joggerst, B., and Simons, K. (1994). Regulated internalization of caveolae. J. Cell Biol. *127*, 1199–1215.

Patterson, G.H., Piston, D.W., and Barisas, B.G. (2000). Forster distances between green fluorescent protein pairs. Anal. Biochem. *284*, 438–440.

Sabharanjak, S., Sharma, P., Parton, R.G., and Mayor, S. (2002). GPI-anchored proteins are delivered to recycling endosomes via a distinct cdc42-regulated, clathrin-independent pinocytic pathway. Dev. Cell *2*, 411–423.

Sharma, P., Sabharanjak, S., and Mayor, S. (2002). Endocytosis of lipid rafts: an identity crisis. Semin. Cell Dev. Biol. *13*, 205–214.

Silvius, J.R. (2003). Role of cholesterol in lipid raft formation: lessons from lipid model systems. Biochim. Biophys. Acta *1610*, 174–183.

Simons, K., and Ikonen, E. (1997). Functional rafts in cell membranes. Nature *387*, 569–572.

Simons, K., and Toomre, D. (2000). Lipid rafts and signal transduction. Nat. Rev. Mol. Cell Biol. *1*, 31–39.

Stryer, L., and Haugland, R.P. (1978). Energy transfer: a spectroscopic ruler. Proc. Natl. Acad. Sci. USA *58*, 719–726.

Subczynski, W.K., and Kusumi, A. (2003). Dynamics of raft molecules in the cell and artificial membranes: approaches by pulse EPR spin labeling and single molecule optical microscopy. Biochim. Biophys. Acta *1610*, 231–243.

Tanaka, F., and Mataga, M. (1979). Theory of time-dependent photoselection in interacting fixed systems. Photochem. Photobiol. *29*, 1091–1097.

Taraboulos, A., Scott, M., Semenov, A., Avrahami, D., Laszlo, L., Prusiner, S.B., and Avraham, D. (1995). Cholesterol depletion and modification of COOH-terminal targeting sequence of the prion protein inhibit formation of the scrapie isoform. J. Cell Biol. *129*, 121–132.

Tsien, R.Y. (1998). The green fluorescent protein. Annu. Rev. Biochem. *67*, 509–544.

Varma, R., and Mayor, S. (1998). GPI-anchored proteins are organized in submicron domains at the cell surface. Nature *394*, 798–801.

Vrljic, M., Nishimura, S.Y., Brasselet, S., Moerner, W.E., and McConnell, H.M. (2002). Translational diffusion of individual class II MHC membrane proteins in cells. Biophys. J. *83*, 2681–2692.

Zacharias, D.A., Violin, J.D., Newton, A.C., and Tsien, R.Y. (2002). Partitioning of lipid-modified monomeric GFPs into membrane microdomains of live cells. Science *296*, 913–916.

Zurzolo, C., van Meer, G., and Mayor, S. (2003). The order of rafts. EMBO Rep. *4*, 1117–1121.